Applied Catalysis A: General 352 (2009) 10–16

Contents lists available at ScienceDirect

Applied Catalysis A: General

journal homepage: www.elsevier.com/locate/apcata

Trimetallic NiMoW unsupported catalysts for HDS

A. Olivas *, D.H. Galván, G. Alonso, S. Fuentes

Centro de Nanociencias y Nanotecnología, Universidad Nacional Autónoma de México, Apdo. Postal 2681, Ensenada, Baja California, Mexico

ARTICLE INFO

Article history:
Received 14 May 2008
Received in revised form 18 September 2008
Accepted 22 September 2008
Available online 5 October 2008

Keywords:
Trimetallic
HDS of DBT
Extended Hückel calculations
DOS
Energy band

ABSTRACT

Trimetallic unsupported NiMoW sulfide catalysts were prepared of by decomposition-sulfidation of bimetallic Mo-W thiosalts precursors impregnated with Ni. The catalytic activity of the catalysts was determined, both *in situ* and *ex situ*, in the dibenzothiophene (DBT) hydrodesulfuration (HDS) reaction. The sample with a relative composition R1 = Mo/[Mo − W] = 0.85 and R2 = Ni/[Mo + W] = 0.5 presented a substantial increment ($k = 23 \times 10^{-7}$ mol/s g) with selectivity to hydrogenation by a factor of 1.24 over hydrodesulfuration. Scanning electron microscopy (SEM) micrographs showed changes in morphology as a function of R1 suggesting that distinct crystalline phases were formed. Also, X-ray diffraction (XRD) measurements of precursors and catalysts revealed that the bimetallic thiosalt structure presents the same planes of the rhombohedral structure as ammonium thiomolybdate (ATM) or ammonium thiotungstate (ATT) indicating that redistribution of Mo and W occurred preferably in specific orientations as the (0 0 2), (0 2 0) and (3 1 0). The ammonium thiomolybdate-thiotungstate (ATMW) bimetallic thiosalt with R1 = 0.85 showed very different structure from the original Mo or W single precursors, among all the samples. Extended Hückel calculations revealed that promotion of (Mo-W)S_2 precursors with Ni forming trimetallic NiMoWS catalysts after sulfidation, increases the availability of electrons over the Fermi level increasing the metallic character of the catalysts.

1. Introduction

New unsupported catalyst called Nebula [1,2], are four times more active than typical hydrodesulphurization (HDS) catalysts and two times more than advanced formulations. Unsupported HDS catalysts were typically prepared by methods such as comaceration [3], homogeneous sulfide precipitation [4] and thiosalt decomposition [5].

The thiosalt decomposition is an interesting alternative preparation since it provides a simple and reproducible method to obtain MoS_2 catalysts with controlled stoichiometry, wide range of surface areas and improved catalytic activity [5–7].

Some patents have reported the use of tetralkylammonium thiometalates to generate carbon-containing MoS_2 and WS_2 catalysts with high surface area and with improved activity [8,9].

The method of in situ decomposition of tetraalkylammonium thiomolybdates in a hydrocarbon solution with sulfur organic compounds and pressurized with hydrogen at 623 K yields active metal sulfide containing carbon at least partly included in the arrangement of the active sites. Such new type of sulfide materials with improved catalytic activity was named amorphous mesoporous sulfide catalysts [10].

Soled et al. [2] have synthesized catalytic trimetallic precursors (Ni-Mo-W) using several methods including direct precipitation and pH controlled precipitation, among others. The recent literature reports that Mo substitution for W partially occurs for precursors containing these two transition metals [10,11]. An amorphous phase is yielded, and catalytic active materials are produced by decomposition and sulfidation.

We report the preparation of trimetallic NiMoW sulfides derived from the impregnation of bimetallic ammonium thiomolybdate-tungstate (ATMW) thiosalts in this work, which are further decomposed *ex situ* or *in situ*. The catalytic activity in the HDS of dibenzothiophene (DBT) and computational calculations using Extended Hückel methods were also analyzed.

2. Experimental

The NiMoW trimetallic sulfide catalysts were obtained by impregnation of $(NH_4)_2$ $(Mo_x\text{-}W_{1-x})$ S_4 bimetallic thiosalts

* Corresponding author. Tel.: +52 646 174 4602x370; fax: +52 646 174 4603.
E-mail addresses: aolivas@cnyn.unam.mx (A. Olivas), galvan@cncyn.unam.mx (D.H. Galván), alonso@cnyn.unam.mx (G. Alonso), fuentes@cnyn.unam.mx (S. Fuentes).

0926-860X/$ – see front matter © 2008 Elsevier B.V. All rights reserved.
doi:10.1016/j.apcata.2008.09.022

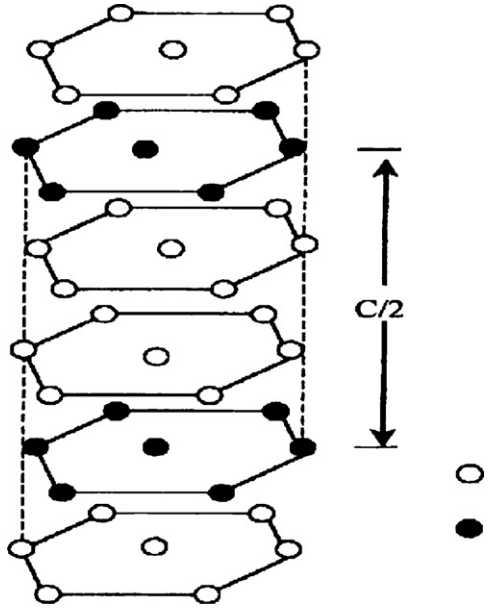

Fig. 1. Unitary cell for 2H- MoS_2. The filled circles are Mo atoms while the open circles are S atoms.

(ATMW) with Ni $(NO_3)_2{\cdot}6(H_2O)$ solutions, according with the ITD method [12]. The bimetallic ATMW complexes were obtained from ammonium heptamolybdate and ammonium metatungstate in ammonia solutions in contact with flowing H_2S gas during 4 h. Three bimetallic thiosalts with Mo/W atomic ratios (R1) = 0.75, 0.85, and 0.95 were prepared. The Ni ratio in the precursors was equal to 0.7 in the first case and constant and equal to 0.5 for the last two cases (R2 = Ni/(Mo + W) ratio). The activation of catalysts was made by treating the NiMoW trimetallic precursor in 15% H_2S/H_2 gas mixtures at 400 C during 4 h.

The resulting precursors and catalysts were placed on the sample holder using highly conductive graphite paint as adhesive to fix the samples and their morphology was studied by scanning electron microscopy (SEM) in a Jeol 5300 microscope, a different magnification settings, operating at 10 kV. Also, X-ray diffraction (XRD) measurements of the samples were made in a Philips diffractometer model X'pert using the Cu Kα radiation (45 kV, 40 mA) with wavelength of 0.154 nm. Interpretation of XRD data was made by comparing experimental patterns with those reported in the ICDD-PDF-2 data bases.

The catalytic activity in the HDS of DBT was evaluated in a batch reactor according to the experimental procedure reported in reference [13].

The calculations reported in this work, have been carried out by means of the tight-binding method [14] within the Extended Hückel [15] framework using YAeHMOP computer package with f-orbitals [16]. The Extended Hückel method is a semi empirical approach for solving Schrödinger equation for a system of electrons, based on the variational theorem. In this approach, explicit electron correlation is not considered except for the intrinsic contributions included in the parameter set. More details about the mathematical formulation of this method have been described elsewhere [17,18] and will be omitted here.

The space group used for calculations of the electronic band structure of Ni(W-Mo)S_2 compounds was the $P6_3/mmc$ (1 9 4) [19], with primitive vectors a = 3.1604 Å and c = 12.2950 Å, as shown in Fig. 1. The band structure calculations for 2H-MoS_2 and 2H-WS_2 were calculated using 37 k points for each case, and sampling the First Brillouin Zone (FBZ).

Fig. 2 depicts the hexagonal Wigner-Seitz cell used in the calculations. Energy was plotted (eV vs. k) ranging from M (1/2 0 0) to Γ(0 0 0) to K (1/3 1/3 0) to M (1/2 0 0) to A (0 0 1/2) to H (1/3 1/3 1/2) of π/a to span the three-dimensional space.

3. Results and discussion

The X-ray diffraction patterns of ATMW precursors are presented in Fig. 3, as a function of the atomic ratio R1. The diffractograms revealed that the bimetallic thiosalt structure presents the same planes of the rhombohedral structure as ATM or ATT but with different intensities, indicating that redistribution of Mo and W occurred preferably in specific orientations as the (0 0 2), (0 2 0) and (3 1 0). The ATMW bimetallic thiosalt with R1 = 0.85 showed the most different structure from the original Mo or W single precursors, of all three samples.

The diffraction patterns of NiMoW sulfided catalysts exhibited only the poorly crystalline structure of (Mo-W)S_2 indicating that a good distribution of nickel was obtained during the impregnation step, as it is possible to observe in Fig. 4. It is suggested that nickel introduction and distribution in the trimetallic precursor was due to the equimolar substitution reaction of ammonium by Ni atoms

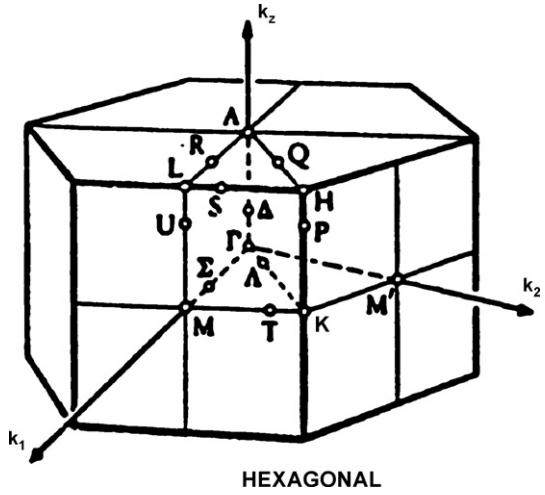

Fig. 2. Wigner-Seitz cell for a hexagonal configuration.

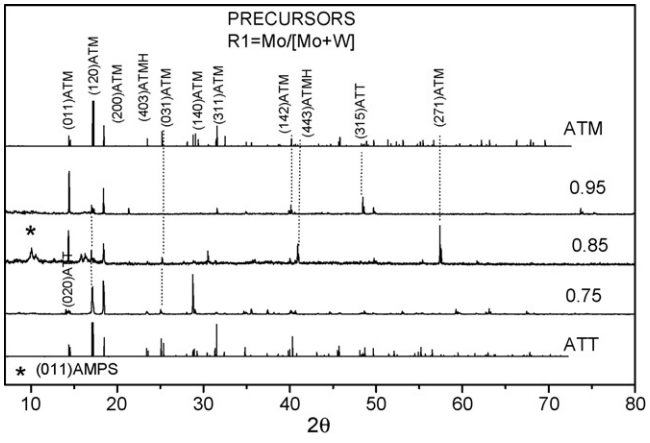

Fig. 3. X-ray diffraction patterns of ATMW thiosalts used as catalysts precursors.

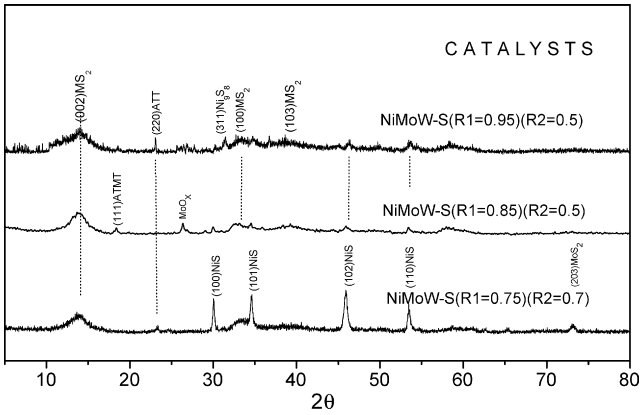

Fig. 4. X-ray diffraction patterns of NiMoW sulfided catalysts after ex situ decomposition.

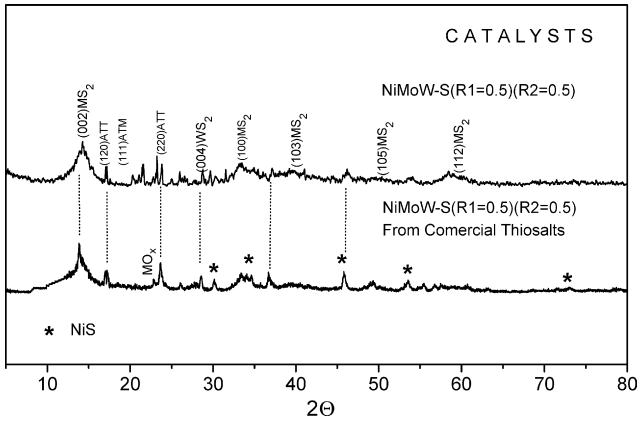

Fig. 5. XRD patterns for catalysts prepared as references. ATT and ATM thiosalts were used to start synthesizing them.

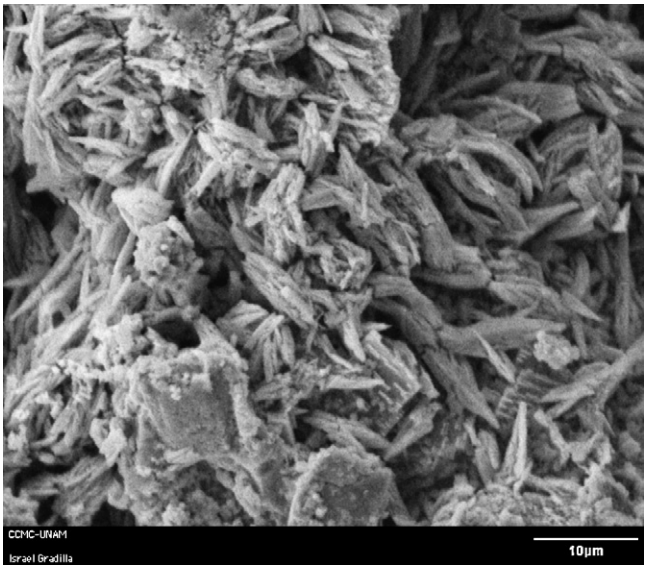

Fig. 7. SEM micrograph of precursor sample with R1 = 0.5.

[11]. No evidence was found about new crystalline sulfide-oxide segregated phases for any R2 value.

Two reference catalysts were prepared, one of them was synthesized by combining ammonium thiomolybdate (ATM) and ammonium thiotungstate (ATT) salts prepared in our laboratory, and in the second one commercial thiosalts were mixed. In both cases we obtained R1 = 0.5 and Ni was added as common with atomic ratio of R2 = 0.5. The analysis by XRD showed fewer impurities as MO_x in the second reference sample from commercial thiosalts but in both cases NiS was segregated as can be observed in Fig. 5.

Comparing all the samples with R2 = 0.5, it was clear that in the ATMW catalysts the nickel is better dispersed, only if an extra amount of Ni is added as on R2 = 0.7, the NiS is mainly detected.

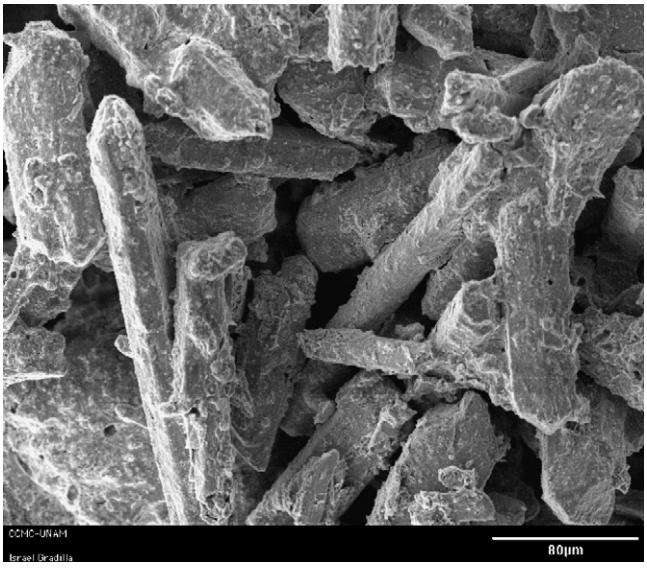

Fig. 6. SEM micrograph of precursor sample with R1 = 0.3.

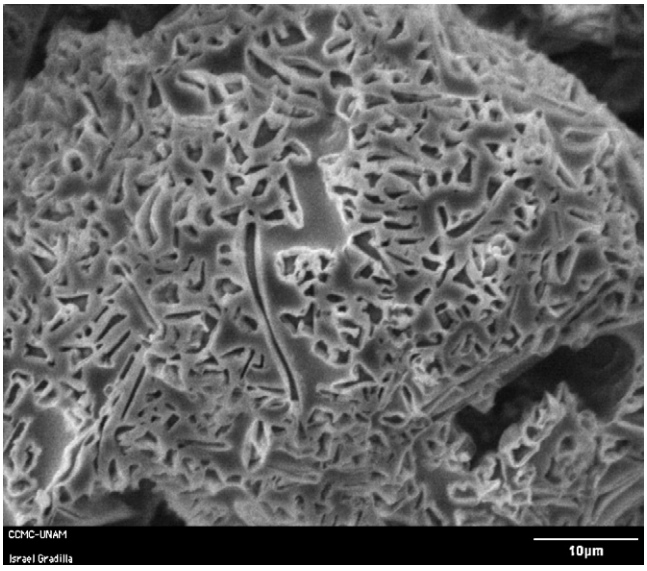

Fig. 8. SEM micrographs of precursor sample with R1 = 0.7.

Table 1
Surface area and steady state catalyst performance in HDS of DBT[a].

Catalyst	Ratio R1, R2	Sa (m^2/g)	*K* specific rate (10^7 mol/s g)	HYD/HDS
Ni-Mo-W *in situ*	0.75, 0.7	19	12.8	0.45
Ni-Mo-W *in situ*	0.85, 0.5	31	12.3	0.59
Ni-Mo-W *in situ*	0.95, 0.5	29	9	0.50
Ni-Mo-W *ex situ*	0.75, 0.7	4	5	1.5
Ni-Mo-W *ex situ*	0.85, 0.5	53	23	1.24
Ni-Mo-W *ex situ*	0.95, 0.5	23	5	1.7
Ni-Mo-W *ex situ* (ref. [1])	0.5, 0.5	26	6	0.97
Ni-Mo-W *ex situ* (ref. [2])	0.5, 0.5	14	14	1.03
Ind Ni-Mo	0.5	150	11	0.5

Ind = $NiMo/Al_2O_3$ industrial.
[a] Batch reactor according to the experimental procedure reported in ref. [13]

Scanning electron microscopy revealed clearly changes in precursor morphology as a function of R1 suggesting that distinct crystalline phases were formed. Faceted rods were observed for the precursor with R1 = 0.75 as shown in Fig. 6, meanwhile other type of morphologies as "smashed wood" in Fig. 7 and "starfish shell" in Fig. 8 were shown for precursors with R1 = 0.85 and 0.75, respectively.

In general, scanning electron microscopy on catalysts before and after reaction only showed single agglomerates and spongy particles not feasible to distinguish one from another, independently of R1, R2.

Surface area results of sulfided catalysts are provided in Table 1, which show an increase for the catalyst with R2 = 0.5 (53 and 23 m^2/g) and a decrease for the catalyst with R1 = 0.75 (4 m^2/g) with respect to (Mo-W)S_2. These results suggest that nickel stabilizes the trimetallic sulfide against sintering by incorporating it in the edge planes of the (Mo-W)S_2 structure.

The nitrogen adsorption–desorption isotherms of sulfided catalysts showed that the adsorbed volume is substantially higher for the Ni(Mo-W)S_2 with R1 = 0.5 presenting a large mesoporosity contribution as can be observed in Fig. 9. The BJH distribution plot of this sample revealed pores in the range 2–16 nm.

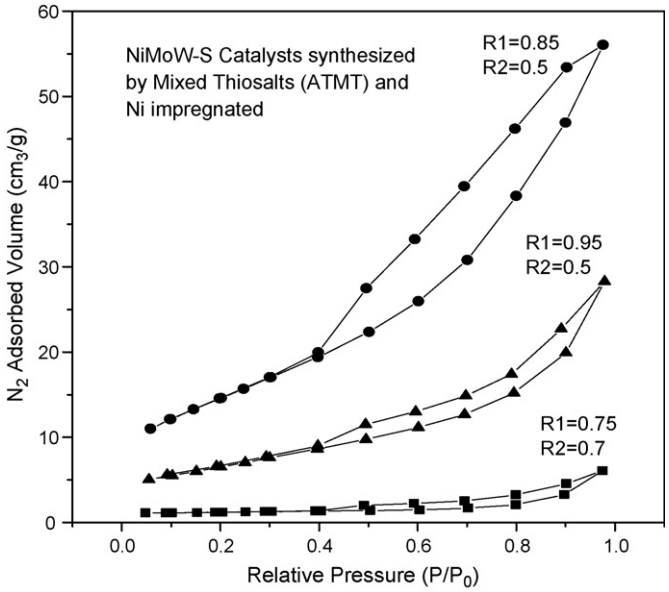

Fig. 9. Nitrogen adsorption–desorption isotherms of the catalysts.

The catalysts were activated both *in situ* and *ex situ*, before the catalytic activity determination. The Ni-Mo-W *ex situ* sample with R1 = 0.85 presented the highest value ($k = 23 \times 10^{-7}$ mol/s g) with selectivity to hydrogenation by a factor of 1.24 over hydrodesulfuration. Catalytic activity results in Table 1 show the highest synergistic effect of Ni for the sample of Ni-Mo-W activated *ex situ* by a factor of ~5. The activity of this catalyst was two times higher than a NiMo/alumina industrial catalyst under the same conditions. It is suggested that the optimum distribution of Ni and W in the MoS_2 poorly crystalline structure of the Ni(Mo-W)S_2 catalyst with R1 = 0.85, is responsible for the good catalytic performance of the catalyst.

The crystalline structure for MoS_2 was made of three hexagonal layers located one at the top of the other layer then the structure is repeated in such a way to form the 2H-MoS_2, see the scheme in Fig. 1, where the black spheres should be the larger atoms or Mo and the white ones are representing the smaller S atoms.

Atomic parameters for Mo and S atoms used in our calculation were obtained from Alvarez [20]. Experimental lattice parameters instead of optimized values were used searching for a best matching of our theoretical results with the available experimental information.

The band structure calculation for the 2H-MoS_2 was calculated using 37 k points sampling the First Brillouin zone (FBZ) as depicted in Fig. 10(a). It is well known that 2H-MoS_2 crystalline bands are split in three sub bands separated by a forbidden gap ranging from 1 to 1.9 eV. These different values were reported by several authors like Mattheiss [21] to Grand et al. [22]. Our calculations yielded indication of this event.

The valence band (VB) is divided in two sub-bands and there is a gap of 2.8 eV (indirect gap between Γ to *K*). The Fermi level is indicated by a horizontal dotted line separating the VB from the CB, as it is observed in Fig. 10(a). Energy in eV *vs.* values were plotted ranging from *M* (1/2 0 0) to Γ (0 0 0) to *K* (1/3 1/3 0) to *M* (1/2 0 0) to *A* (0 0 1/2) to *H* (1/3 1/3 1/2) of π/a to span the three-dimensional space as depicted in Fig. 10. In order to form the new structure Mo-W-S, we started from MoS_2 when one of the site of the Mo was substituted for W arriving to the final configuration $Mo_{(1-x)}W_{(x)}S_2$. The energy bands corresponding to this new structure are depicted in Fig. 10(b). Notice that this new system becomes metallic due that the Fermi level is located within several bands. This behavior could be attributed to the extra electrons that W provides to the unitary cell. Moreover, it is possible to identify that some of the bands became multiply degenerate due to the contribution of the extra electrons provided from W. This analysis will be expanded when we shall explain the projected Density of States for this structure in the following section.

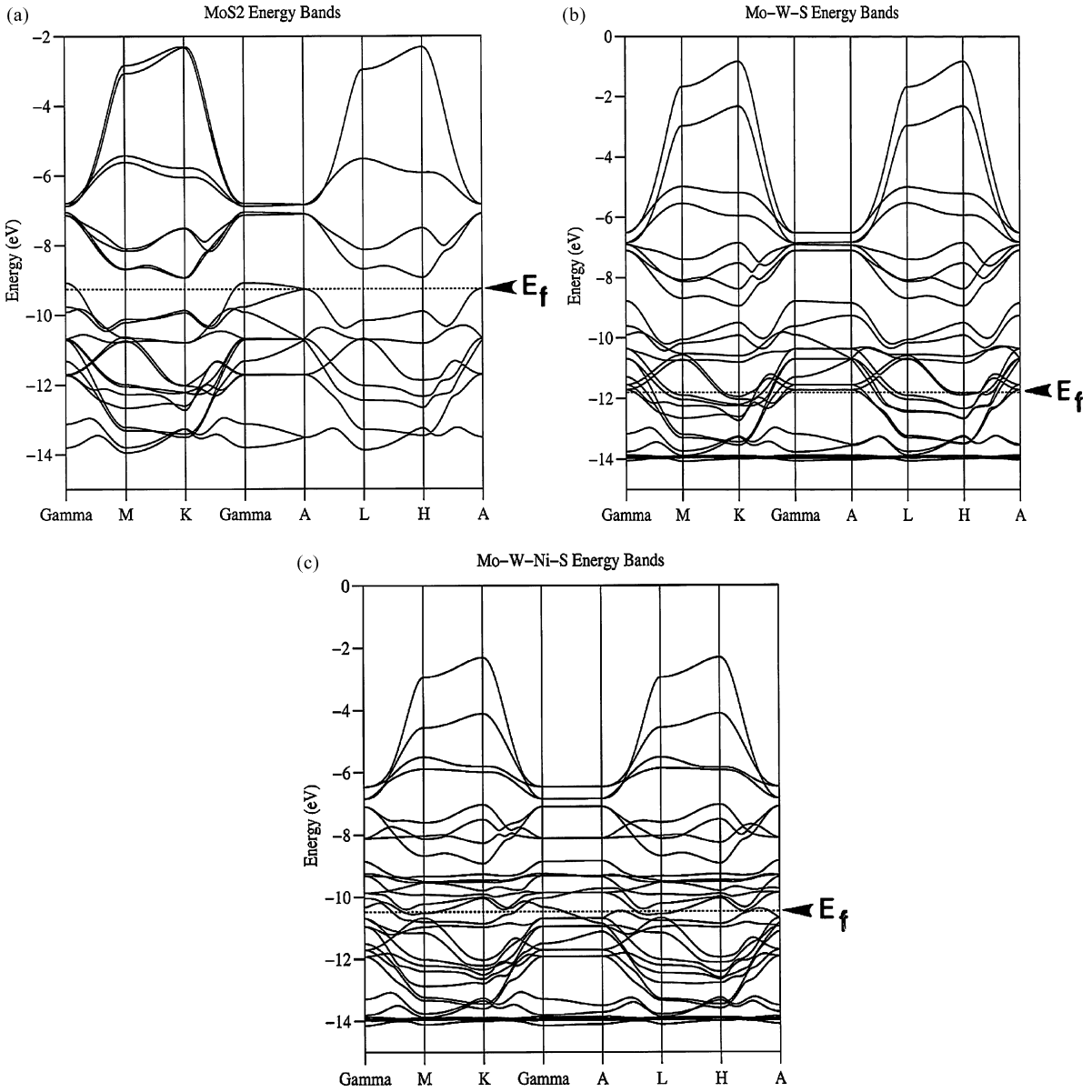

Fig. 10. (a) Energy bands for MoS_2. (b) Energy bands for (Mo-W)S_2. (c) Energy bands for Ni (Mo-W)S_2, where Ni atoms are located on the top of the layer.

In order to form the Mo-W-Ni-S structure, to the former structure we located randomly some Ni atoms at the top the S layer. The results are provided in Fig. 10(c). Again, notice that the new system continues to be metallic.

Total and projected Density of States (PDOS) for MoS_2, $Mo_{(1-x)}W_{(x)}S_2$ and $Mo_{(1-x)}W_{(x)}NiS_2$ are depicted in Fig. 11(a)–(c), respectively. Fig. 11(a) depicts total DOS, while the hatched dotted line is the selected projected DOS for each orbital of the selected atoms in the unit cell. The horizontal dotted line indicates the Fermi level.

In each graph total and PDOS are shown vs. % composition selecting the highest peak as 100% and the other peaks are scaled in proportion to that specific peak. The PDOS for Mo d- and S p-orbitals is provided and indicated with big arrows for each case separately. Notice for the other cases, also indicated by arrows are Mo d-, W *d*-, Ni p- and S p-orbitals. Notice and overall resemblance with another reports but in order to be more careful searching for a possible hybridization (overlap between orbitals), we pay attention to those contributions near the Fermi level. From Fig. 11(a), Mo d- contributes with ≅5% while S p-orbitals contribute ≅2% to the total DOS.

In the case related to $Mo_{(1-x)}W_{(x)}S_2$, Fig. 11(b), Mo d-orbitals contribute with ≅3%, W d-orbitals contribute with ≅2% and S p-orbitals contribute with ≅15% of the total DOS. Notice an increase in the contribution of S when compared to MoS_2. This is a clear indication of how W promotes that the new system is more likely to be metallic, as shown in the energy bands. Furthermore, when we analyze $Mo_{(1-x)}W_{(x)}$ NiS_2 the situation is not so different than the case we analyze formerly, due that Mo d-orbitals contribute with ≅3%, W contribute with ≅3%, Ni p-orbitals with ≅2% and S p-orbitals contribute with ≅15% to the total DOS. This behavior promotes that the system becomes more metallic when the Ni is located randomly on the surface of one of the S layers.

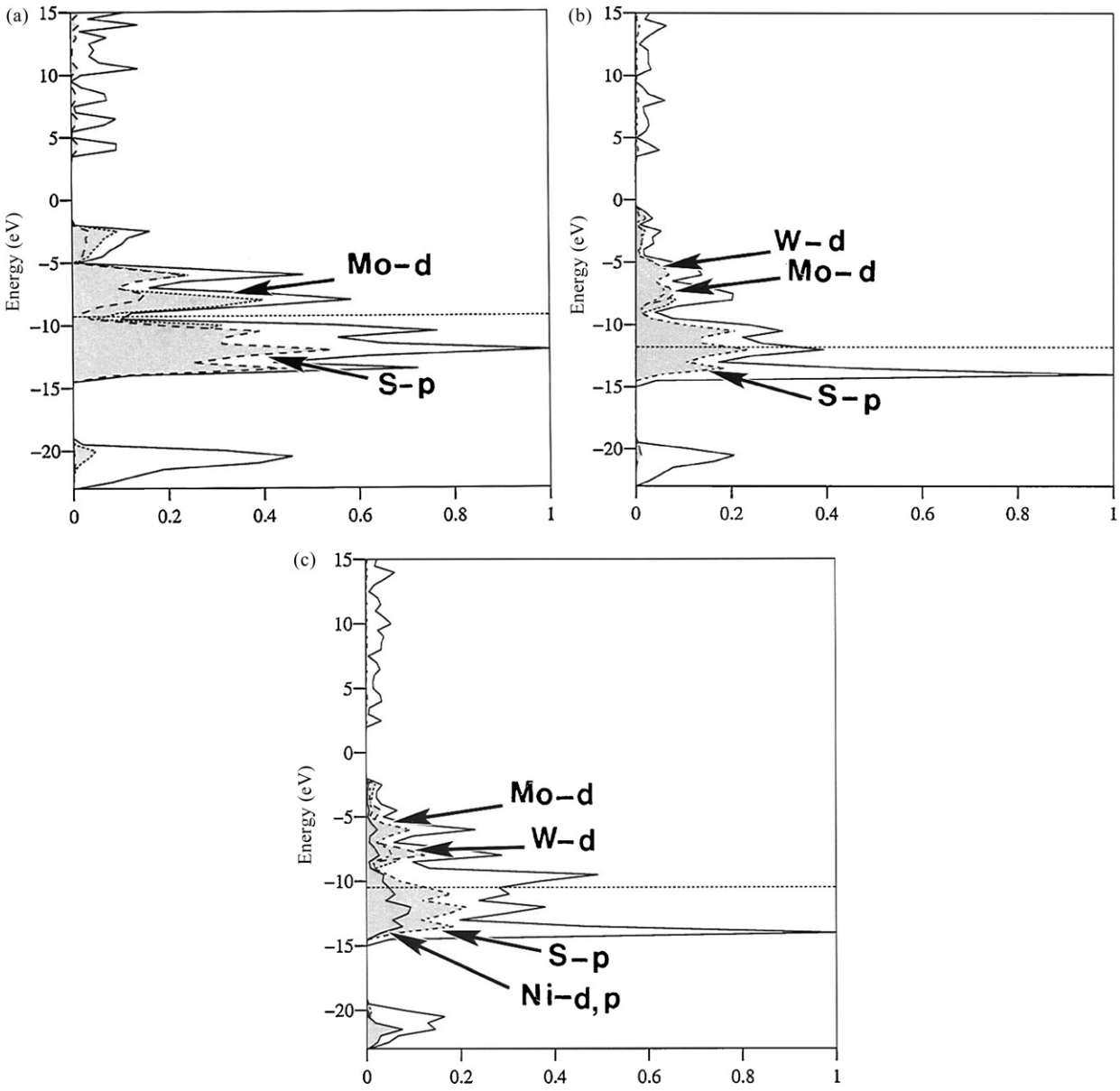

Fig. 11. (a) Total and projected density of states about the Fermi level for MoS_2, (b) for (Mo-W)S_2 and (c) for Ni(Mo-W)S_2, where Ni is on the top of the layer.

4. Conclusions

The trimetallic NiMoW sulfide catalysts with R1 = 0.85 and prepared by the impregnation of bimetallic ATMW thiosalts yield very promising unsupported catalysts with good Ni distribution, adequate mesoporosity, significant synergistic effect and two times more activity (in a weight basis) than an industrial NiMo/alumina catalysts. The optimal composition and distribution of atoms in the precursor obtained by controlling the reactions occurring during the preparation steps yielded a very active catalyst. By this means, the synergistic effect of Ni is higher in (Mo-W)S_2 than in Ni(MoS_2) and Ni(WS_2) separated. Such a behavior is attributed to the formation of metallic states in the Ni-Mo-W-S catalyst due to the electronic interaction of Mo with W and Ni as show Extended Hückel calculations.

According to these calculations, the combination of Mo and W atoms in forming binary (Mo-W)S_2 compounds changes the semiconductor character of MoS_2 or WS_2 increasing the metallic character. The addition of Ni to form trimetallic Ni(Mo-W)S_2 compounds additionally increases the availability of electrons over the Fermi level. However, we believe that the position of Ni in the structure determines, or is a determining factor to the magnitude of the effect. We are doing additional work to observe the contribution of Ni to the metallic character when it is located at the border of the structure rather than on top of the sulfur atoms.

From the energy bands for MoS_2, a clear indication that the system is semiconductor with an E_g of 2.8 eV between the CB and the VB. On the other hand, the energy bands for the new systems $Mo_{(1-x)}W_{(x)}S_2$ and $Mo_{(1-x)}W_{(x)}NiS_2$ indicate that both systems are metallic.

Total and projected DOS provided information regarding the contributions of each atom to the appropriate DOS in a specific energy range. In this manner, it was possible to detect an overlap (hybridization) in the vicinity of the Fermi level for MoS_2, $Mo_{(1-x)}W_{(x)}S_2$ and $Mo_{(1-x)}W_{(x)}NiS_2$. This hybridization becomes stronger as Ni particles were located at the surface of the S-layer.

The results obtained corroborate experimental findings that the catalytic activity could be correlated to the existence of the metallic edges of the MoS_2 clusters decorated with S atoms [23] at the top of the sulfur layer and suggest a direct way to tailor catalysts.

The band electronic structure calculations of MoS_2 revealed that the valence band (VB) is divided in two sub-bands and there is a gap of 2.8 eV (indirect) from *H* to *A* (Fig. 10(a)). The Fermi level (E_f) appears between the valence and the conduction band confirming that MoS_2 is a semiconductor. Similar results were obtained for WS_2.

Calculations of density of states at the Fermi level shows that Mo 3d and S 2p orbitals overlap at the Fermi level, as shown in Fig. 11(a). This result indicates that hybridization of the s, p and d orbitals occurs in MoS_2 as well as in WS_2.

The band electronic structure calculations of (Mo-W)S_2 compounds show that the conduction band presents a higher density of electronic states than MoS_2 or WS_2 (Fig. 10(b)). In this case the Fermi level appears in the conduction band indicating that we have now a metallic behavior instead of a semiconductor. The DOS at the Fermi level of this compound shows a higher density of electronic states than MoS_2 or WS_2 (Fig. 11(b)). The Mo 4d, W 5d and S 2p orbitals overlap the Fermi level indicating that hybridization of orbitals from Mo and W occurs.

The band electronic structure calculations of Ni(Mo-W)S_2 compounds, where Ni is located on top, over the sulfur atoms shows that the Fermi level appears at the same place in the conduction band confirming that we have a metallic behavior similar to (Mo-W)S_2. In this case the VB and CB bands do not overlap as in the previous case. Nevertheless, the conduction band shows a higher density of electronic states compared to (Mo-W)S_2. For this case, the Mo 4d, W 5d, 3d of Ni and S 2p orbitals overlap the Fermi level indicating that hybridization of orbitals occurred.

Acknowledgments

The authors are grateful to E. Flores, F. Ruiz, G. Vilchiz (CCMC), and C. Ornelas (CIMAV) for technical assistance. For economical support to the grants from PAPIIT-UNAM IN119602-3 and IN104105-2, from Conacyt P-46735-Y.

References

[1] F.L. Plantenga, R.G. Leliveld, Appl. Catal. A 248 (2003) 1.
[2] S.L. Soled, S. Miseo, R. Krikak, H. Vroman, T.H. Ho, K.L. Riley, US Patent 6,299,760 B1 (2001) (to Exxon Research and Engineering Company).
[3] G. Hagenbach, P. Courty, B. Delmon, J. Catal. 31 (1973) 264.
[4] R. Candia, B.S. Clausen, H. Topsoe, J. Catal. 77 (1982) 564.
[5] M. Zdrazil, Catal. Today 3 (1988) 269.
[6] S. Fuentes, G. Díaz, F. Pedraza, H. Rojas, N. Rosas, J. Catal. 113 (1988) 535.
[7] A.W. Naumann, A.S. Behan, U.S. Patent 4,243,554 (1981) (to Union Carbide Corporation).
[8] T.A. Pecoraro, R.R. Chianelli, U.S. Patent 4,528,089 (1985) (to Exxon Research and Eng. Co.).
[9] R.R. Chianelli, A.J. Jacobson, U.S. Patent 4,650,563 (1987) (to Exxon Research and Eng. Co.).
[10] G. Alonso, M.H. Siadati, G. Berhault, A. Aguilar, S. Fuentes, R.R. Chianelli, J. Catal. 208 (2002) 359.
[11] M. Nath, K. Mukhopadhyay, C.N.R. Rao, Chem. Phys. Lett. 352 (2002) 163.
[12] A. Olivas, M. Avalos, S. Fuentes, Mater. Lett. 43 (2000) 1–5.
[13] A. Olivas, G. Alonso, S. Fuentes, Top. Catal. 39 (2006) 175.
[14] M.-H. Whangbo, R. Hoffmann, J. Am. Chem. Soc 100 (1978) 6093.
[15] R. Hoffmann, J. Chem. Phys. 39 (1963) 1397.
[16] G.A. Landrum, W. Glassey, The YAeHMOP (1999) is freely available on www at URL: http://overlap.chem.Cornell.edu:8080/yaehmop.html.
[17] D.H. Galván, J. Mater. Sci. Lett. 17 (1998) 805.
[18] W.V. Glassey, G.A. Papoian, R. Hoffmann, J. Chem. Phys. 111 (1999) 893.
[19] P.D. Fleischauer, J.R. Lence, P.A. Bertrand, R. Baner, Langmuir 5 (1985) 1009.
[20] S. Alvarez, Tables of Parameters for Extended Hückel Calculations, Universitat de Barcelona, Barcelona, March 1993, p. 121.
[21] L.F. Mattheiss, Phys. Rev. B 8 (1973) 3719.
[22] A.J. Grand, T.M. Griffiths, G.D. Pitt, A.D. Yoffe, J. Phys. C: Solid State Phys. 8 (1975) L17.
[23] D.H. Galvan, A. Posada-Amarillas, J.C. Samaniego-Reyna, G.A. Camacho-Bragado, M.J. Yacamán, Curr. Top. Catal., in press.